

Two-Phase Master Sintering Curve for 17-4 PH Stainless Steel



IM DOO JUNG, SANGYUL HA, SEONG JIN PARK, DEBORAH C. BLAINE,
RAVI BOLLINA, and RANDALL M. GERMAN

The sintering behavior of 17-4 PH stainless steel has been efficiently characterized by a two-phase master sintering curve model (MSC). The activation energy for the sintering of gas-atomized and water-atomized 17-4 PH powders is derived using the mean residual method, and the relative density of both powders is well predicted by the two-phase MSC model. The average error between dilatometry data and MSC model has been reduced by 68 pct for gas-atomized powder and by 45 pct for water-atomized powder through the consideration of phase transformation of 17-4 PH in MSC model. The effect of δ -ferrite is considered in the two-phase MSC model, leading to excellent explanation of the sintering behavior for 17-4 PH stainless steel. The suggested model is useful in predicting the densification and phase change phenomenon during sintering of 17-4 PH stainless steel.

DOI: 10.1007/s11661-016-3687-0

© The Minerals, Metals & Materials Society and ASM International 2016

I. INTRODUCTION

THE grade 17-4 PH stainless steel is a precipitation hardening martensite stainless steel with high strength and good corrosion resistance. Due to these advantages, 17-4 PH stainless steel has been widely used in medical, automotive, aircraft, and military applications. Exceptionally high tensile strength with moderate ductility is obtained by the combination of solid solution hardening, precipitation strengthening, and phase transformation from austenite to martensite during heat treatment. This alloy, however, has low machinability, and the conventional processing methods are only limited to simple shape components. Therefore, particulate material (PM) manufacturing methods have been actively studied and applied to this alloy. For example, powder injection molding, a near-net shape manufacturing technology, is known to easily fabricate 17-4 PH stainless steel to full density.^[1–6]

Sintering is a thermally activated process used to manufacture PM. Densification *via* sintering is associated with a volume change (shrinkage) governed by the conservation of mass. It is critical to the PM manufacturer to monitor and control the concomitant

densification and shrinkage to produce quality materials within specified density and dimensional limits. To this end, various sintering models have been proposed over the past decades.^[7–27] One of the simplest and most functional models is the master sintering curve (MSC), originally developed by Su and Johnson.^[28] The MSC approach has served as the foundation for a number of studies aimed at modeling the sintering process for various PM material systems.^[29–43]

The MSC approach is used to predict sintering densification by considering one sintering mechanism to be dominant and persistent over the entire sintering cycle. For many of the PM systems that have been studied, this is an appropriate assumption.^[36,37,41–43] However, 17-4 PH stainless steel exhibits different sintering behaviors at different temperatures, dependent on the phases that appear during sintering.^[24,44–46] These phase changes have been confirmed by a study of the microstructural evolution during sintering of powder injection-molded 17-4 PH stainless steel.^[47] This study indicates 17-4 PH stainless steel powder is martensitic at room temperature, and as such, this is the phase of the injection-molded sample at lower temperatures of sintering. The martensite transforms into γ -austenite around 993 K (700 °C), which correlates to the relevant phase diagram shown in Figure 1(a). A second phase transformation, γ -austenite to δ -ferrite, starts around 1473 K (1200 °C). The percentage of δ -ferrite in the microstructure as a function of temperature is shown in Figure 1(b).^[48] Additionally, these studies elucidate the influence that the different diffusivities associated with each phase have on densification by noting the change in linear shrinkage rate with temperature.

In this study, a two-phase master sintering curve is developed and linearized by relating the natural logarithm of the work-of-sintering to the densification

IM DOO JUNG, Postdoctoral Researcher, and SEONG JIN PARK, Professor, are with the Department of Mechanical Engineering, Pohang University of Science and Technology, San 31, Hyojadong, Nam-gu, Pohang 790-784, Republic of Korea. Contact e-mail: sjpark87@postech.edu SANGYUL HA, Principal Research Engineer, is with Samsung Electro-Mechanics, Mayoung-Ro 150, Suwon, Republic of Korea. DEBORAH C. BLAINE, Professor, is with the Department of Mechanical and Mechatronics Engineering, Stellenbosch University, Matieland 7602, South Africa. RAVI BOLLINA, Professor, is with the School of Engineering Sciences, Mahindra Ecole Centrale, Hyderabad, Telangana, India. RANDALL M. GERMAN, Professor, is with the Mechanical Engineering Department, San Diego State University, San Diego, CA 92182.

Manuscript submitted June 10, 2015.

Article published online August 12, 2016

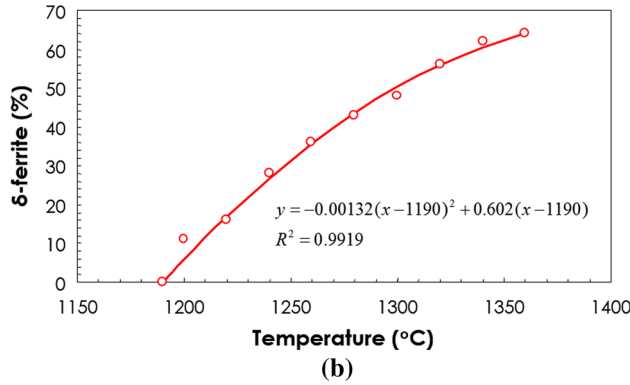
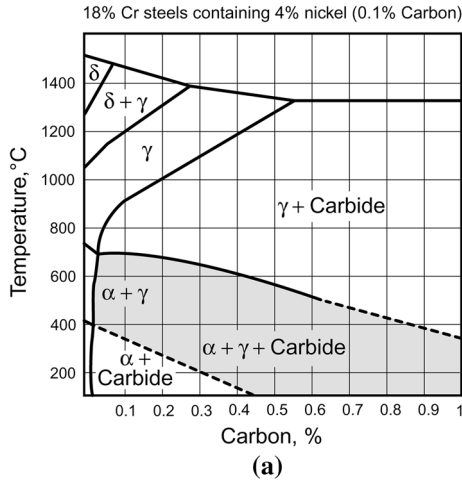


Fig. 1—(a) Phase diagram of 18 pct Cr steel containing 4 pct nickel (0.1 pct carbon) and (b) amount of δ -ferrite with function of temperature.

parameter. Water-atomized and gas-atomized powders were compared for their sintering behavior analysis and characterized by two-phase master sintering curve.

II. MASTER SINTERING CURVE THEORY

The MSC was originally developed by Su and Johnson,^[28] derived from Coble's combined stage sinter model.^[15] The details of the model are fully explained in a number of publications.^[28–36] Blaine *et al.* presented a mathematical manipulation of the sigmoid function that typically fits the model well, offering a linearized version of the MSC.^[49] The linearized MSC is formulated by relating the densification ratio, Φ , to the work-of-sintering, θ . The densification ratio represents a relative progression in sintering densification, defined as

$$\Phi \equiv \frac{\rho - \rho_0}{1 - \rho_0}. \quad [1]$$

The relative density at the onset of sintering densification is ρ_0 , relating to a densification ratio $\Phi = 0$; once full density has been reached, the relative density, ρ , is unity and delivers an associated densification ratio of $\Phi = 1$. The work-of-sintering is an integral over the

sintering thermal cycle, defined by the time t at temperature T , expressed as

$$\theta(t, T) = \int_{t_0}^t \frac{1}{T} \exp\left(-\frac{Q}{RT}\right) dt, \quad [2]$$

where Q is the apparent activation energy for sintering densification and R is the Universal gas constant. The thermal events occurring during sintering occur simultaneously, and some do not induce densification; therefore, the activation energy is called “apparent” as it only gives an empirical indication of the temperature dependence of sintering densification by concomitant diffusional mechanisms.

The linear MSC relates these two parameters to each other as follows:

$$\ln \Phi = n \ln\left(\frac{\theta}{\theta_{\text{ref}}}\right), \quad [3]$$

where n is the power law exponent (from the nonlinearized form of Eq. [3]) and θ_{ref} is the value of the work-of-sintering midway through densification, at $\rho = (\rho_0 + 1)/2$.^[49]

Typically, an iterative procedure is employed for determining the apparent activation energy for sintering densification; this usually involves minimization of a mean residual error between the predictive curve and experimental data.^[22,28,29] Sometimes, especially for single-phase, solid-state sintering, where the primary diffusional mechanism for sintering is known, the published activation energy for the volume or grain boundary diffusion, as appropriate, is used.^[34] In most of these cases, the iterative value for Q is very close to the theoretical value.^[35] In this study, as there are a few phases that appear over the sintering cycle for 17-4 PH stainless steel, the iterative method is used. The calculation of the mean residual is determined by the equation suggested by Blaine *et al.*,^[49] repeated here for convenience:

$$\text{Mean residual} = \sqrt{\frac{1}{\rho_f - \rho_0} \int_{\rho_0}^{\rho_f} \sum_{i=1}^N \frac{\left(\frac{\theta_i}{\theta_{i\text{-avg}}} - 1\right)^2}{N} d\rho}, \quad [4]$$

where ρ_f is the final relative density, N is total number of dilatometry tests, i is the dummy variable for summation, θ_i is the work-of-sintering at i th value of relative density, and $\theta_{i\text{-avg}}$ is the average value of the work-of-sintering up to i th value of density. Integration over the relative density instead of the work-of-sintering range gives more accurate and efficient convergence to a minimum value of the mean residual while iterating for Q . The power law exponent, n , is equivalent to the slope of the linear MSC in Eq. [3]:

$$n \equiv \frac{d \ln \Phi}{d \ln \theta}. \quad [5]$$

The equivalence given in Eq. [5] is particularly useful when constructing a MSC for material systems, such as 17-4 PH stainless steel, where the diffusion rate changes over the course of sintering due to the presence or transformation of different phases. The slope of the linear MSC will change accordingly and multiphase MSCs can be constructed to more accurately model sintering densification over the entire sintering cycle. This study illustrates this concept through application to the sintering of injection-molded 17-4 PH stainless steel.

III. EXPERIMENTAL PROCEDURES

In this study, we use two different 17-4 PH stainless steel powders with D50 particle size of 10 μm to illustrate and verify the proposed two-phase MSC: gas-atomized 17-4 PH stainless steel powder and water-atomized 17-4 PH stainless powder. The melting temperature and theoretical density of 17-4 PH stainless steel are 1677 K to 1713 K (1404 $^{\circ}\text{C}$ to 1440 $^{\circ}\text{C}$) and 7.73 g/cm^3 .^[48] We have used a vertical pushrod dilatometer (Anter Laboratories Unitherm model #1161, Anter Laboratories, Pittsburgh, PA) capable of measuring sintering shrinkage, shrinkage rate, and furnace chamber temperature *in situ*. The measured pycnometer density of both 17-4 PH stainless steel powders was 7.64 g/cm^3 . To prepare samples for dilatometry test, feedstocks were formulated using both types of 17-4 PH powder with a water-based agar binder system in 55 powder volume percent, injection molded into a bar-shape mold and debound in 873 K (600 $^{\circ}\text{C}$) furnace flowing H_2 gas removing binders. Oil quenching method and Archimedes method were used to measure the densities of samples. The algorithm for constructing a two-phase MSC is summarized in Figure 2.

The MSC is characterized by a series of constant heating rate or isothermal hold sintering experiments. For the gas-atomized powder, six different dilatometry tests were conducted, as described in Table I. Tests A, B, and C ramp up from room temperature to a first holding temperature of 1283 K (1010 $^{\circ}\text{C}$) at a heating rate of 10 K ($^{\circ}\text{C}$)/min; thereafter, the tests ramp up to a second hold temperature of 1638 K (1365 $^{\circ}\text{C}$) using different heating rates for each test. Tests D and E have a same holding temperature at 1473 K (1200 $^{\circ}\text{C}$) and ramp up to this temperature at different heating rates for each test, and F has the highest hold temperature of 1673 K (1400 $^{\circ}\text{C}$) with same heating rate with E. Three dilatometry tests were conducted for water-atomized powder, as described in Table II. All three tests had two different holding temperatures, ramping from room temperature to the first holding temperature at a heating rate of 10 K ($^{\circ}\text{C}$)/min and then from the first to the second holding temperature with a heating rate of 1.67 K ($^{\circ}\text{C}$)/min. All tests, for both the gas- and water-atomized powders, were conducted in a vertical pushrod dilatometer capable of recording sintering shrinkage, shrinkage rate, and furnace chamber temperature *in situ*. This dilatometer is regularly calibrated to a sapphire standard for

accuracy and repeatability of shrinkage and temperature measurement. The experimental data collected from the dilatometer are then used to calculate the sintering densification by subtracting the thermal expansion from the linear shrinkage, assuming isotropic shrinkage for the volume, and relating the volume change to the density change with the assumption of constant sample mass. Therefore, the sintered density at any point in the sintering cycle can be calculated, and these data are used to construct a MSC.

The dilatometry data can also be used to identify phase changes that are associated either with volumetric changes or with changes in shrinkage rates because of altered diffusion rates of varying phases.

IV. RESULTS AND DISCUSSION

A. Phase Changes

In Figure 3, the shrinkage and shrinkage rate from Test F are shown. The shrinkage rate curve shows a peak at 993 K (720 $^{\circ}\text{C}$), indicating the volume change associated with the phase change from original α' -martensite to γ -austenite. The shrinkage increases with a change to the shrinkage slope at 1263 K (990 $^{\circ}\text{C}$), which indicates the onset of densification. This is similar to the behavior noted by other researchers.^[47] From 1383 K to 1473 K (1110 $^{\circ}\text{C}$ to 1200 $^{\circ}\text{C}$), the shrinkage rate plateaus, indicating the maximum shrinkage rate of the γ -austenite single phase. Finally, at 1473 K (1200 $^{\circ}\text{C}$), the shrinkage slope changes, indicating onset temperature for the second phase for master sintering curve. This temperature coincides with the appearance of δ -ferrite on the γ -austenite grains, indicating the onset of a dual phase microstructure for the 17-4 PH stainless steel microstructure.^[42]

For gas-atomized powder, the calculated constant thermal expansion coefficient from dilatometry data during cooling is $2.14 \times 10^{-5} \text{K}^{-1}$ with error of 5.58 pct. For water-atomized powder, the calculated constant thermal expansion coefficient from dilatometry data during cooling is $1.37 \times 10^{-5} \text{K}^{-1}$ with error of 7.50 pct.

B. Activation Energy of MSC

In Figure 4, the mean residual of activation energy is shown for gas-atomized powder and water-atomized powder. For gas-atomized powder, the calculated apparent activation energy [$T \leq 1473 \text{K}$ (1200 $^{\circ}\text{C}$)] was 321 kJ/mol by minimizing residual based on MSC with residual of 0.185. The apparent activation energy [$T > 1473 \text{K}$ (1200 $^{\circ}\text{C}$)] was 350 kJ/mol by minimizing residual based on MSC with residual of 0.269. For water-atomized powder, the calculated apparent activation energy [$T \leq 1473 \text{K}$ (1200 $^{\circ}\text{C}$)] was 349 kJ/mol by minimizing residual based on MSC with residual of 0.110. The apparent activation energy [$T > 1473 \text{K}$ (1200 $^{\circ}\text{C}$)] was 360 kJ/mol by minimizing residual based on MSC with residual of 0.0959.

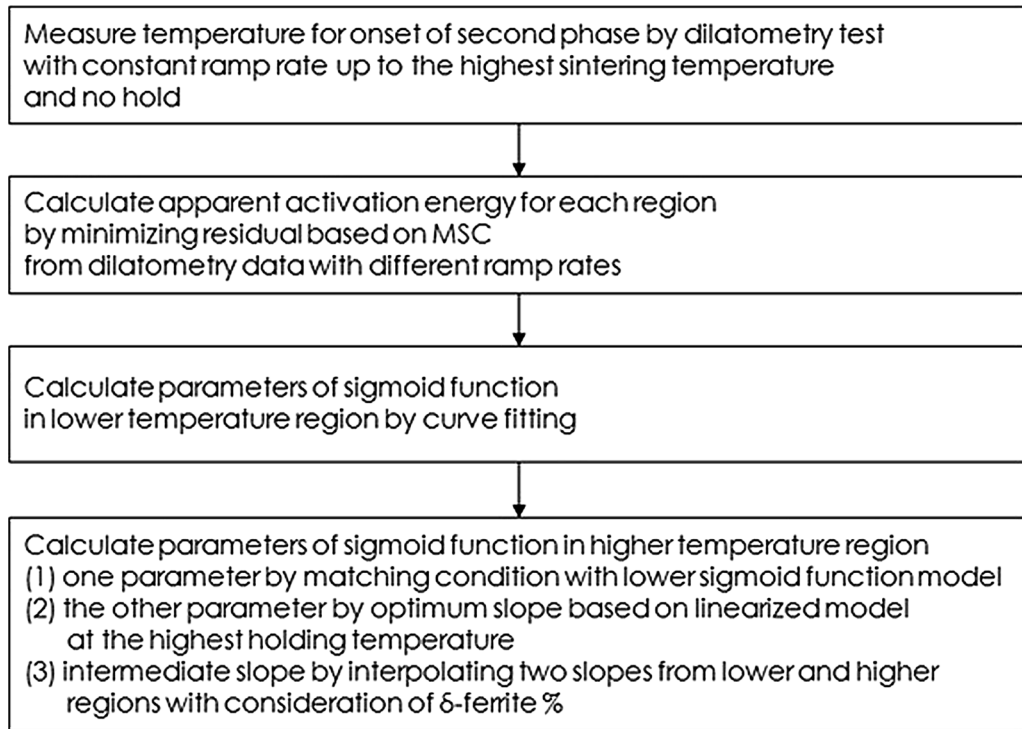


Fig. 2—Overall algorithm for constructing two-phase MSC of 17-4 PH stainless steel.

Table I. Dilatometry Test Condition for Gas-Atomized Powder

Test	Ramp 1 (K/min)	Hold 1	Ramp 2 (K/min)	Hold 2	Cool (K/min)
A	10	1283 K (1010 °C) 1 h	7	1638 K (1365 °C) 1 h	10
B	10	1283 K (1010 °C) 1 h	5	1638 K (1365 °C) 1 h	10
C	10	1283 K (1010 °C) 1 h	1.67	1638 K (1365 °C) 1 h	10
D	7	1473 K (1200 °C) 1 h	—	—	10
E	5	1473 K (1200 °C) 1 h	—	—	10
F	5	1673 K (1400 °C) 1 h	—	—	10

Table II. Dilatometry Test Condition for Water-Atomized Powder

Test.	Ramp 1 (K/min)	Hold 1	Ramp 2 (K/min)	Hold 2	Cool (K/min)
A	10	1200 K to 1473 K (927 °C to 1200 °C) no hold	1.67	1603 K (1330 °C) 1 h	10
B	10	1283 K (1010 °C) 1 h	1.67	1638 K (1365 °C) 1 h	10
C	10	1283 K (1010 °C) 1 h	1.67	1603 K (1330 °C) 1 h	10

C. MSC Without the Consideration of Phase Change

The master sintering curves for both types of powder without the consideration of phase change are shown in Figure 5. A nondimensional relative density value has been employed, which is 1 for full density. For gas-atomized powder, the function of relative density can be written as below:

$$\rho_s = 0.55 + \frac{0.45}{1 + \exp\left(-\frac{(\ln \theta + 29.93)}{1.521}\right)}, \quad [6]$$

where the activation energy, 350 kJ/mol [$T > 1473$ K (1200 °C)], was used in the calculation because

densification below 1473 K (1200 °C) was relatively small compared with densification above 1473 K (1200 °C). The sigmoid function model in Eq. [6] had average error of 1.34 pct and maximum error of 8.70 pct. For water-atomized powder, the function of relative density is written as below:

$$\rho_s = 0.55 + \frac{0.45}{1 + \exp\left(-\frac{(\ln \theta + 30.41)}{1.890}\right)}, \quad [7]$$

where the activation energy 360 kJ/mol was used with the same reason of gas-atomized powder. The Eq. [7] had average error of 1.06 pct and maximum error of 6.26 pct.

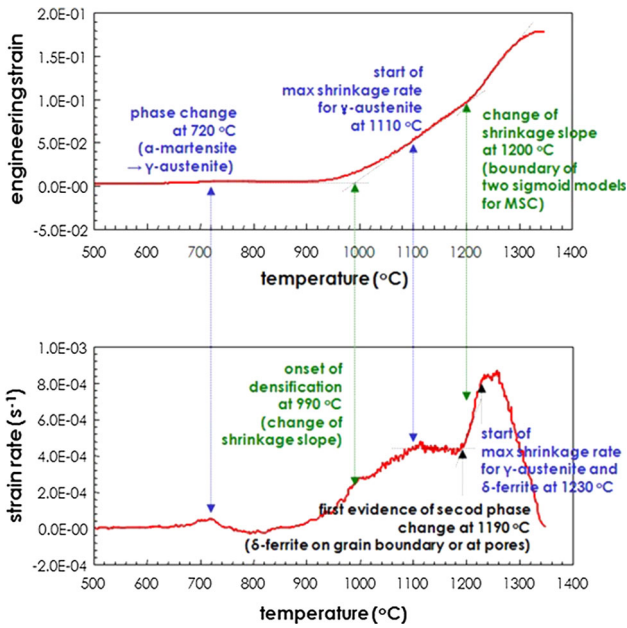


Fig. 3—Shrinkage and shrinkage rate from Exp. F in Table I.

D. MSC with the Consideration of Phase Change

In Figure 6, the MSCs and linearized model for both powders considering phase change are shown. For the gas-atomized powder at $T \leq 1473$ K (1200 °C), the relative density function is given below:

$$\rho_s = 0.55 + \frac{0.45}{1 + \exp\left(-\frac{(\ln \Theta + 26.48)}{2.006}\right)} \quad [8]$$

This model had average error of 0.826 pct and maximum error of 3.44 pct. In logarithmic linearized form, this MSC model is as follows:

$$\ln \Phi = \frac{1}{2.006} (\ln \Theta + x), \quad [9]$$

where x is -26.28 , the halfway to full density, and the density difference ratio Φ is defined below:

$$\Phi = \frac{\rho - 0.55}{1.0 - \rho} \quad [10]$$

For the temperature above 1473 K (1200 °C), the two-phase MSC is written as below:

$$\rho_s = 0.55 + \frac{0.45}{1 + \exp\left(-\frac{(\ln \Theta + x)}{0.09512}\right)}, \quad [11]$$

where the average error is 0.211 pct and maximum error is 0.411 pct, which is much less than the MSC model without the consideration of phase change. The linearized two-phase MSC model is as follows:

$$\ln \Phi = \frac{1}{0.09512} (\ln \Theta + x), \quad [12]$$

where x is dependent of sintering cycle and the value is -27.09 for Exp. A, -26.91 for Exp. B, and -26.16 for Exp. C.

For water-atomized powder at $T \leq 1473$ K (1200 °C), the two-phase MSC model is given as follows:

$$\rho_s = 0.55 + \frac{0.45}{1 + \exp\left(-\frac{(\ln \Theta + 29.45)}{2.035}\right)} \quad [13]$$

The average error and maximum error were 0.750 and 1.54 pct, respectively. The linearized model is given below:

$$\ln \Phi = \frac{1}{2.035} (\ln \Theta + x) \quad [14]$$

where x is -29.25 , the halfway to full density. For the temperature $T > 1473$ K (1200 °C), the two-phase MSC model is written as below:

$$\rho_s = 0.55 + \frac{0.45}{1 + \exp\left(-\frac{(\ln \Theta + x)}{0.4428}\right)} \quad [15]$$

which had the average error of 0.338 pct and the maximum error of 0.932 pct. The linearized form of Eq. [15] is written as below:

$$\ln \Phi = \frac{1}{0.4428} (\ln \Theta + x), \quad [16]$$

where x is dependent of sintering cycle and its value is -28.13 for Exp. A, -28.79 for Exp. B, and -29.23 for Exp. C.

The consideration of phase changes in two-phase master sintering curve with different activation energies in different phases reduced 68 pct of average error for gas-atomized powder and 45 pct of average error for water-atomized powder from the single-phase master sintering curve. The detailed comparisons of measured densities and the predicted relative densities are summarized in Tables III and IV.

E. Comparison of Two Powders

In Figure 7, the relative density profile for the two experimental powders (gas and water-atomized 17-4 PH powder) was compared under the same dilatometry conditions. Gas-atomized 17-4 PH powder reached full density faster than water-atomized 17-4 PH powder, while two types of powder have the same D50 size of 10 μm . This phenomenon is in accordance with the general faster sintering behavior of spherically shaped gas-atomized powder, which has larger surface area to receive heat affection than that of less spherically shaped water-atomized powder. Water atomization process has much less time to spheroidize in comparison to gas atomization.^[50] This relationship between surface area and fast sintering behavior is employed efficiently in spark plasma sintering process using nanosized powder to enhance fast diffusion paths for mass transport provided by significant volume fraction of interface.^[51–54] Comparison of the two-phase MSCs of these

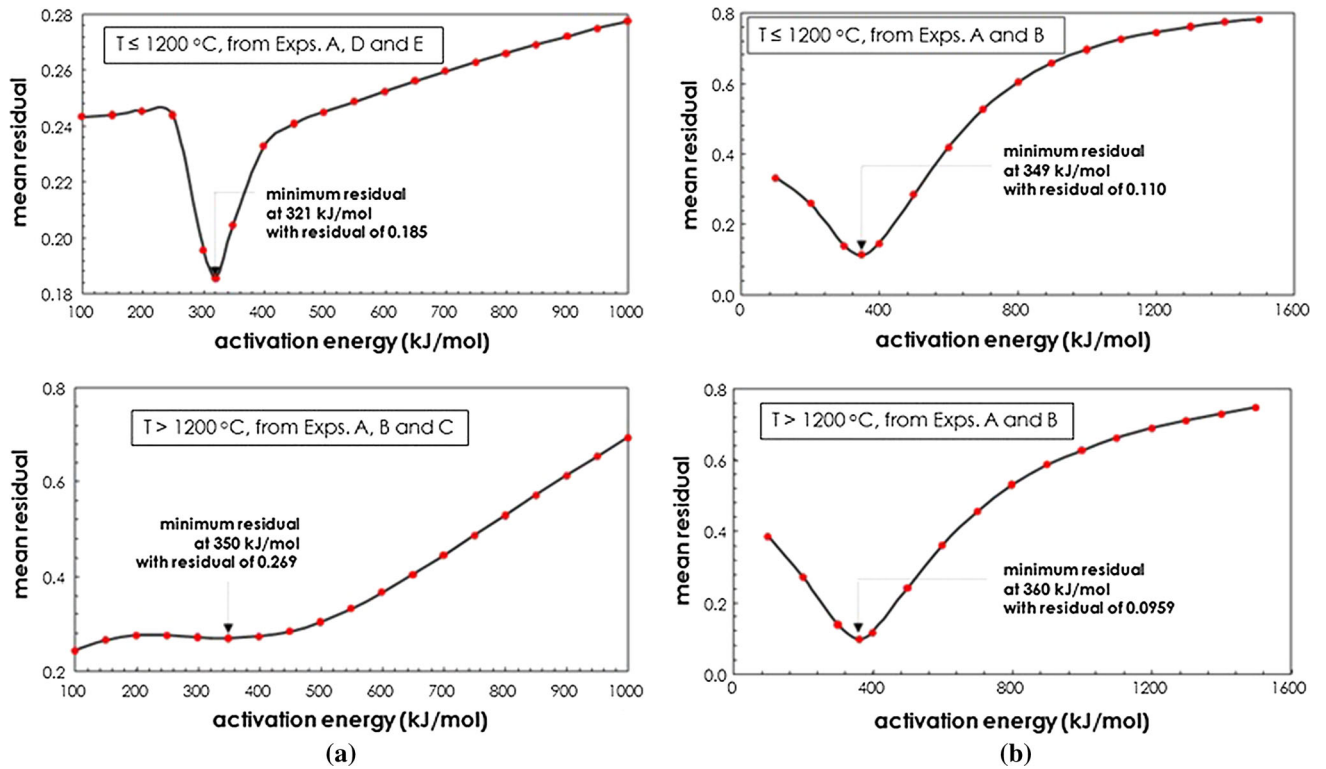


Fig. 4—Determining apparent activation energies: (a) gas-atomized and (b) water-atomized.

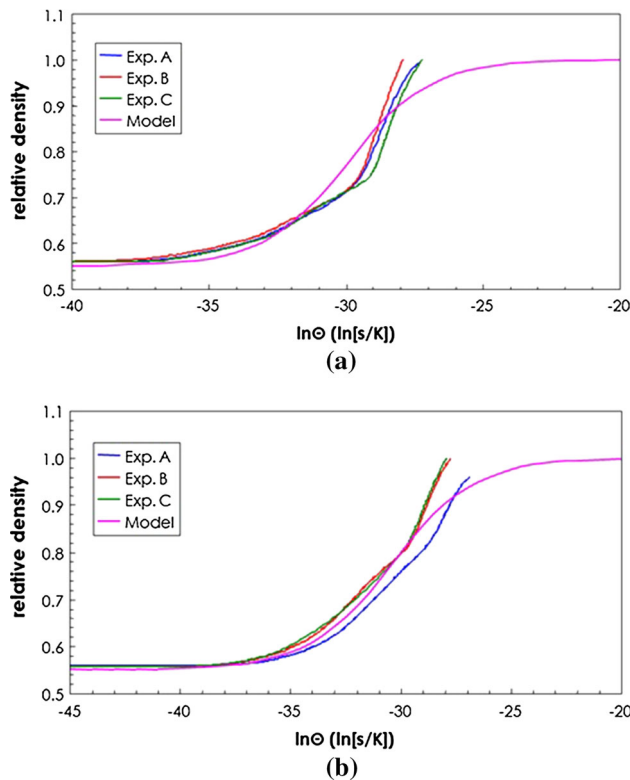


Fig. 5—MSCs without the consideration of phase change: (a) gas-atomized and (b) water-atomized.

powders is shown in Figure 8. One can see the relative density changes with significant phase change behavior of two powders shown in Figure 8(a). This difference can be quantified by comparing the first linearized density values of second phase for two powders, -28.78 for water-atomized powder, and -26.16 for gas-atomized powder. Their time–temperature–density relationships are summarized in Figure 9.

F. Two-Phase MSC with the Consideration of Amount of δ -Ferrite

As shown in Eq. [17], first slope parameter for lower sigmoid function model is obtained from the slope of lower linearized model region ($1/2.006$).

$$\ln \Phi = \frac{1}{2.006} (\ln \Theta + 26.48) [T \leq 1190 \text{ K } (917^\circ \text{C})]. \quad [17]$$

Similarly, the second slope parameter is obtained from highest holding temperature ($1/0.01641$). Finally, the intermediate slope can be obtained by interpolating two slope values from lower and higher regions with consideration of δ -ferrite. With the consideration of δ -ferrite, the linearized model can be written as below:

$$\ln \Phi_{i+1} = \ln \Phi_i + \left(\frac{1 - \delta}{2.006} + \frac{\delta}{0.01641} \right) \times (\ln \Theta_{i+1} - \ln \Theta_i) [T > 1463 \text{ K } (1190^\circ \text{C})], \quad [18]$$

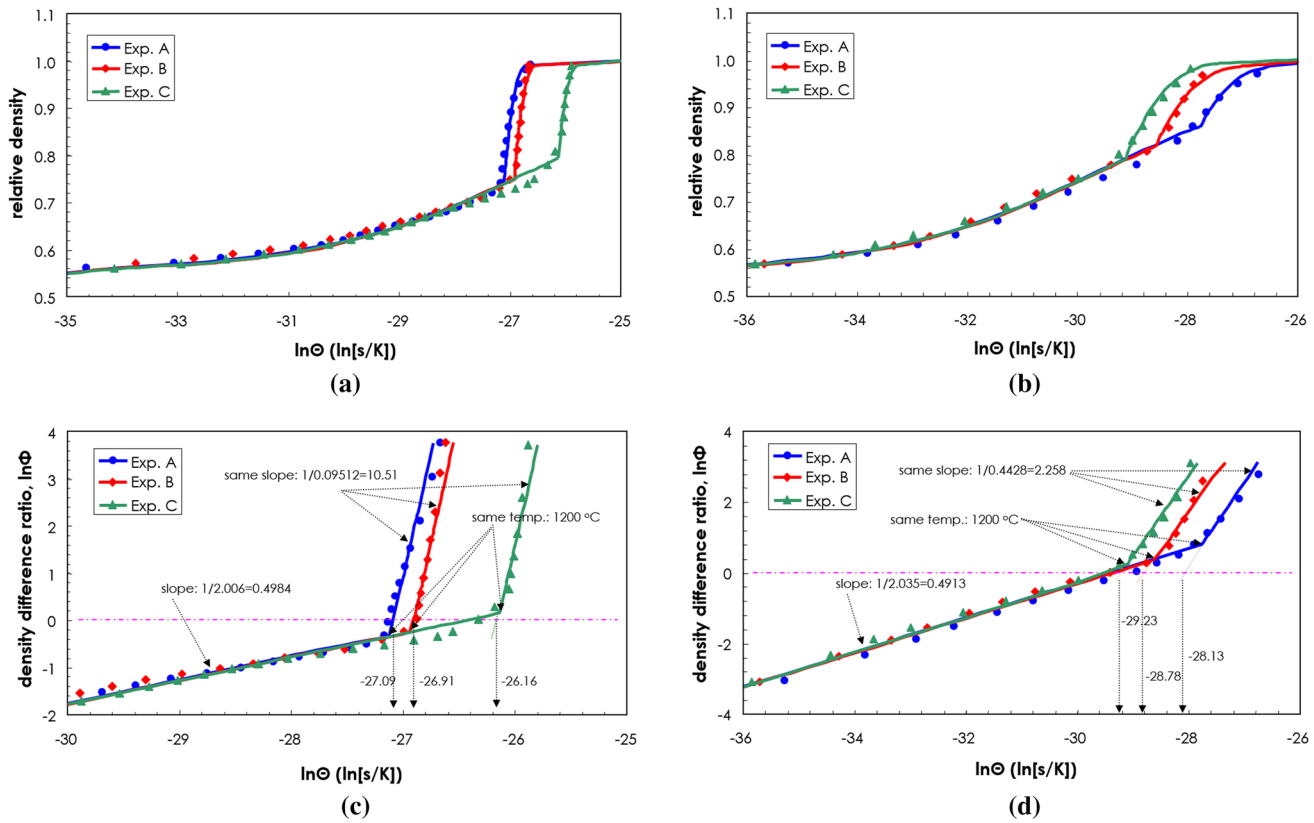


Fig. 6—MSCs with the consideration of phase change: (a) gas-atomized, (b) water-atomized, (c) linearized MSC for gas-atomized, and (d) linearized MSC water-atomized.

Table III. Comparison of Measured and Predicted Densities for Gas-Atomized Powder

Exp.	Sintered Relative Density				
	Archimedes	MSC Without Phase Change		MSC With Phase Change	
		Density	Error (Percent)	Density	Error (Percent)
A	0.831	0.877	5.46	0.828	0.44
B	0.889	0.943	6.09	0.896	0.75
C	0.961	0.958	0.35	0.964	0.30
D	0.967	0.981	1.47	0.983	1.70
E	0.981	0.988	0.71	0.993	1.23
Average Error (Percent)		2.82		0.89	

Table IV. Comparison of Measured and Predicted Densities for Water-Atomized Powder

Exp.	Quenching Point	Sintered Relative Density				
		Archimedes	MSC Without Phase Change		MSC with Phase Change	
			Density	Error (Percent)	Density	Error (Percent)
A	final	0.982	0.973	0.92	0.999	1.73
B	1283 K (1010 °C)/after 1 h	0.699	0.613	12.3	0.661	5.37
	1373 K (1100 °C)/no hold	0.728	0.677	5.97	0.729	0.10
	1473 K (1200 °C)/no hold	0.838	0.830	0.96	0.831	0.78
	1573 K (1300 °C)/no hold	0.963	0.946	1.77	0.959	0.38
	1638 K (1365 °C)/no hold	0.973	0.964	0.92	0.992	1.95
	1638 K (1365 °C)/after 1 h	0.982	0.982	0.02	0.999	1.73
	final	0.992	0.982	1.01	0.999	0.74
C	final	0.988	0.973	1.48	0.999	1.16
Average Error (Percent)			2.82		1.55	

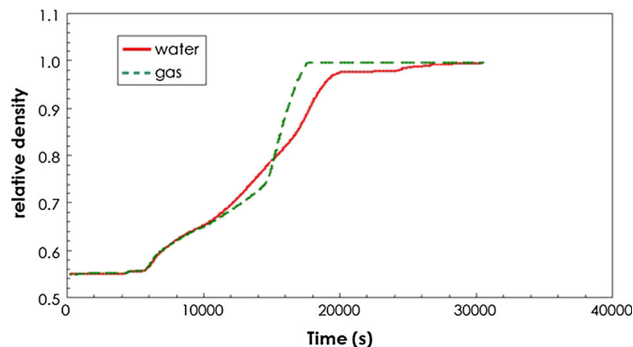


Fig. 7—Dilatometry plots of two powders with the same sintering cycle (Exp. C for gas-atomized and Exp. B for water-atomized).

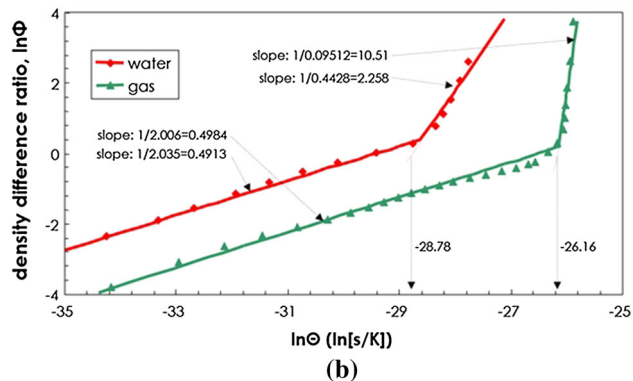
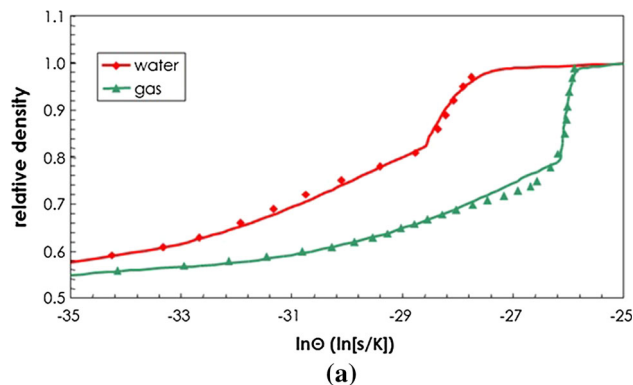


Fig. 8—MSC plots of two powders with the same sintering cycle (Exp. C for gas-atomized and Exp. B for water-atomized): (a) MSC plot and (b) linearized MSC plot.

where δ is the content of δ -ferrite and defined as below:

$$\delta = (\delta_i + \delta_{i+1}/2). \quad [19]$$

In Figure 10, the two-phase models considering the amount of δ -ferrite were compared with the two-phase model without this consideration for Exps. A, B, and C. The δ -ferrite considered models have the average error of 0.116 pct and maximum error of 0.335 pct, which are further reduced compared to those of two-phase MSCs without the consideration of the δ -ferrite.

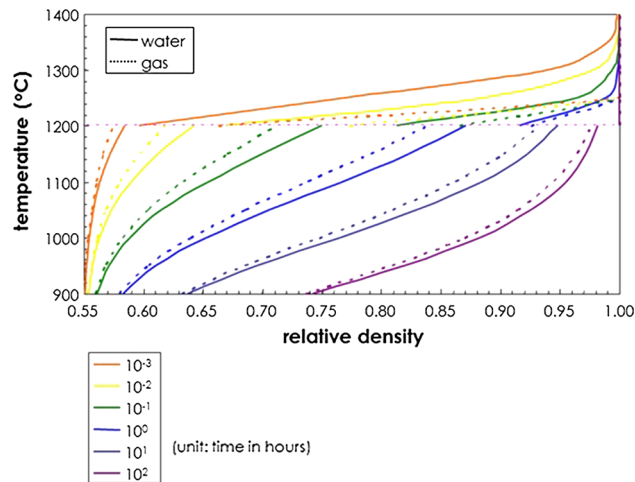


Fig. 9—Time-temperature-density diagram of two powders.

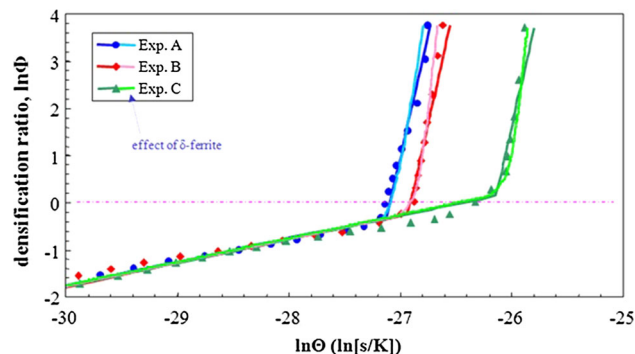


Fig. 10—Temperature profile (Exp. A) and corresponding densities for gas-atomized powder.

V. CONCLUSIONS

The sintering behavior of 17-4 PH stainless powder is successfully characterized by the two-phase MSC model. The activation energies for sintering densification of gas-atomized and water-atomized 17-4 PH powders were 321 and 349 kJ/mol. The relative density of 17-PH has been well predicted by the two-phase MSC model with the average error of 0.826 pct for gas-atomized powder and 0.750 pct for water-atomized powder. The consideration of the amount of δ -ferrite in gas-atomized powder has reduced the average error further to 0.116 pct. The numerical models obtained in this work are very useful for the accurate analysis of 17-4 PH sintering behavior and the optimization of cycles to reach various technical goals related to the time, temperature, heating rate, and similar processing parameters.

ACKNOWLEDGMENT

This work was supported by the National Research Foundation of Korea (NRF) Grant funded by the Korean government (NRF-2010-0026242/2011-0030075).

REFERENCES

1. J.J. Valencia, T.J. McCabe, and H. Dong: in *Advances in Powder Metallurgy and Particulate Materials*, vol. 6, M. Philips and J. Porter, eds., Metal Powder Industries Federation, Princeton, 1995, pp. 205–212.
2. T. Baba, H. Miura, T. Honda, and Y. Tokuyama: *Adv. Powder Metall. Part. Mater.*, 1995, vol. 6, p. 271.
3. R.M. German and D. Kubish: *Int. J. Powder Metall.*, 1993, vol. 29, p. 47.
4. Y. Wu, R.M. German, D. Blaine, B. Marx, and C. Schlaefel: *J. Mater. Sci.*, 2002, vol. 37, p. 3573.
5. H. Zhang and R.M. German: *Proceedings of The 1992 Powder Injection Molding Symposium*, Metal Powder Industries Federation, Princeton, NJ, 1992, p. 219.
6. K. Kamada, M. Nakamura, and H. Horie: *Proceedings of 2000 Powder Metallurgy World Congress*, Kyoto, Japan, 2000, p. 1021.
7. R.L. Coble: *J. Appl. Phys.*, 1961, vol. 32, pp. 787–92.
8. V.V. Skorohod: *Rheological Basis of the Theory of Sintering*, Naukova Dumka, Kiev, 1972.
9. G.C. Kuczynski: *Mater. Sci. Monogr.*, 1981, vol. 8, pp. 44–52.
10. S. Helle, K.E. Easterling, and M.F. Ashby: *Acta Metall.*, 1985, vol. 33, pp. 2163–74.
11. M.N. Rahaman, L.C. De Jonghe, and R.J. Brook: *J. Am. Ceram. Soc.*, 1986, vol. 69, pp. 53–58.
12. R.K. Bordia and G.W. Scherer: *Acta Metall.*, 1988, vol. 36, pp. 2393–97.
13. M.F. Ashby: *Background Reading HIP 6.0*, University of Cambridge, Cambridge, UK, 1990.
14. J. Besson and M. Abouaf: *Acta Metall. Mater.*, 1991, vol. 39, pp. 2225–34.
15. J.D. Hansen, R.P. Rusin, M.-H. Teng, and D.L. Johnson: *J. Am. Ceram. Soc.*, 1992, vol. 75, pp. 1129–35.
16. R.M. McMeeking and L.T. Kuhn: *Acta Metall. Mater.*, 1992, vol. 40, pp. 961–69.
17. Z.-Z. Du and A.C.F. Cocks: *Acta Metall. Mater.*, 1992, vol. 40, pp. 1969–79.
18. Z.-Z. Du and A.C.F. Cocks: *Acta Metall. Mater.*, 1992, vol. 40, pp. 1981–94.
19. Y.S. Kwon, G. Son, J. Suh, and K.T. Kim: *J. Am. Ceram. Soc.*, 1994, vol. 77, pp. 3137–41.
20. Y.S. Kwon and K.T. Kim: *ASME J. Eng. Mater. Technol.*, 1996, vol. 118, pp. 448–55.
21. K. Darcovich, L. Bera, and K. Shinagawa: *Mater. Sci. Eng. A*, 2003, vol. 341, pp. 247–55.
22. R.M. German: *Sintering Theory and Practice*, Wiley, New York, 1996.
23. S.J.L. Kang and Y.I. Jung: *Acta Mater.*, 2004, vol. 52, pp. 4573–78.
24. Y.S. Kwon, Y. Wu, P. Suri, and R.M. German: *Metall. Mater. Trans.*, 2004, vol. 35A, pp. 257–63.
25. E.A. Olevsky, V. Tikare, and T.J. Garino: *J. Am. Ceram. Soc.*, 2006, vol. 89, pp. 1914–22.
26. S. He and J. Ma: *Mater. Sci. Eng. A*, 2006, vol. 361, pp. 1914–22.
27. M.W. Reiterer, K.G. Ewsuk, and J.G. Arguello: *J. Am. Ceram. Soc.*, 2006, vol. 89, pp. 1930–35.
28. H. Su and D.L. Johnson: *J. Am. Ceram. Soc.*, 1996, vol. 79, pp. 3211–17.
29. M.-H. Teng, Y.-C. Lai, and Y.-T. Chen: *West. Pac. Earth Sci.*, 2002, vol. 2, pp. 171–80.
30. K. An and D.L. Johnson: *J. Mater. Sci.*, 2002, vol. 37, pp. 4555–59.
31. T.R.G. Kuttly, K.B. Khan, P.V. Hegde, J. Banerjee, A.K. Sengupta, S. Majumdar, and H.S. Kamath: *J. Nucl. Mater.*, 2004, vol. 327, pp. 211–19.
32. K.G. Ewsuk, D.T. Ellerby, and C.B. DiAntonio: *J. Am. Ceram. Soc.*, 2006, vol. 89, pp. 2003–09.
33. S. Kiani, J. Pan, and J.A. Yeomans: *J. Am. Ceram. Soc.*, 2006, vol. 89, pp. 3393–96.
34. D.C. Blaine, J.D. Gurosik, S.J. Park, D.F. Heaney, and R.M. German: *Metall. Mater. Trans.*, 2006, vol. 37A (3), pp. 715–20.
35. D.C. Blaine, S.J. Park, P. Suri, and R.M. German: *Metall. Mater. Trans.*, 2006, vol. 37A, pp. 2827–35.
36. S.J. Park, J.M. Martin, J.F. Guo, J.L. Johnson, and R.M. German: *Metall. Mater. Trans.*, 2006, vol. 37A, pp. 2837–48.
37. S.J. Park, J.M. Martin, J.F. Guo, J.L. Johnson, and R.M. German: *Metall. Mater. Trans.*, 2006, vol. 37A, pp. 3337–43.
38. P. Garg, S.-J. Park, and R.M. German: *Int. J. Refract. Met. Hard Mater.*, 2007, vol. 25, pp. 16–24.
39. S.J. Park and R.M. German: *Int. J. Mater. Struct. Integr.*, 2007, vol. 1, pp. 128–47.
40. D. Li, S. Chen, W. Shao, X. Ge, Y. Zhang, and S. Zhang: *Mater. Lett.*, 2008, vol. 62, pp. 849–51.
41. S.J. Park, S.H. Chung, J.M. Martín, J.L. Johnson, and R.M. German: *Metall. Mater. Trans.*, 2008, vol. 39A, pp. 2941–48.
42. R.M. German, P. Suri, and S.J. Park: *J. Mater. Sci.*, 2009, vol. 44, pp. 1–39.
43. R. Bollina, S.J. Park, and R.M. German: *Powder Metall.*, 2010, vol. 53, pp. 20–26.
44. J.W. Newkirk, J.A. Sago, and G.M. Brasel: *Processing and Fabrication of Advanced Materials*, The Minerals, Metals and Materials Society, Warrendale, PA, 1998 213.
45. H. Kyogoku, S. Komatsu, H. Nakayama, H. Jinushi, and K. Shinohara: *Advances in Powder Metallurgy and Particulate Materials*, Metal Powder Industries Federation, Princeton, NJ, 1997, vol. 3, p. 18.
46. K.A. Green: *Advances in Powder Metallurgy and Particulate Materials*, Metal Powder Industries Federation, Princeton, NJ, 1998, vol. 2, p. 5.
47. Y. Wu, D. Blaine, B. Marx, C. Schlaefel, and R.M. German: *Metall. Mater. Trans. A*, 2002, vol. 33, pp. 2185–94.
48. D. Peckner and I.M. Bernstein: *Handbook of Stainless Steels*, 1977, Mc Graw-Hill, USA.
49. D. Blaine, S.J. Park, and R.M. German: *J. Am. Ceram. Soc.*, 2009, vol. 92, pp. 1403–09.
50. P.C. Angelo and R. Subramanian: *Powder Metallurgy: Science, Technology and Applications*, Prentice-Hall of India Pvt. Ltd, New Delhi, 2008, vol. 10, pp. 228–29.
51. A.S. Sharma et al.: *Mater. Metall. Trans. A*, 2011, vol. 42A (7), pp. 2071–84.
52. A.S. Sharma: *J. Mater. Res.*, 2013, vol. 28 (11), pp. 1517–28.
53. G.B. Raju et al.: *Scr. Mater.*, 2009, vol. 61 (7), pp. 674–77.
54. G.B. Raju et al.: *Scr. Mater.*, 2009, vol. 61 (1), pp. 104–07.